



Factorial design analysis of As(V) adsorption onto iron-aluminum binary oxide-doped clinoptilolite

Esra Bilgin Simsek^{a,b,*}, Ercan Özdemir^c, Asli Ozge Avcı Tuna^a, Ulker Beker^a

^aChemical Engineering Department, Yıldız Technical University, Davutpasa—Esenler, Istanbul 34210, Turkey
Tel. +902123834755; Fax: +902123834725; email: esrabilgin622@gmail.com

^bChemical and Process Engineering Department, Yalova University, Yalova 77100, Turkey

^cClean Energy and Nanotechnology Research Center, Gebze Institute of Technology, Gebze, Kocaeli 41400, Turkey

Received 4 March 2013; Accepted 17 July 2013

ABSTRACT

Arsenic adsorption onto an iron-aluminum binary oxide-doped clinoptilolite was studied by using response surface methodology. The Box–Behnken experimental design was used to estimate the effects of major process parameters, namely pH (3–7), temperature (25–65 °C), and initial arsenate (As(V)) concentration (0.5–9.5 mg L⁻¹). The experimental data fitted to the empirical second-order model was found to be significant, as was evident from the model *F*-value of 341.23. The coefficient of determination value of second-order regression model was found to be 0.9977 ($R_{adj} = 0.9948$), indicating the accuracy and general availability of the model. The initial arsenic concentration of 9.4 mg L⁻¹, pH of 6.0, and temperature of 62.4 °C were found to be optimum for maximum As(V) uptake. The results showed that adsorption capacity increased with increasing temperature, indicating the endothermic nature of the adsorption process.

Keywords: Arsenic; Binary oxides; Box–Behnken; Response Surface Methodology

1. Introduction

The introduction of arsenic into water sources by natural or anthropogenic activities can lead to health, environmental, and ecological effects due to its high toxicity [1]. Long-term exposure to arsenic via water sources could cause cardiovascular, neurological, and respiratory diseases, skin lesions, and bladder, lung, skin and other cancers [2]. As arsenic affects human health, novel adsorbents, such as iron, aluminum, manganese, and titanium oxides, have been developed to remove the arsenic present in water/wastewater [3]. Combinations of these oxides possess a high

potential for water remediation due to their combined properties like affinity, chemical stability, low cost, and nontoxicity [4–7]. Distribution of arsenic is handled by iron and aluminum oxides in most oxidized environments. Combined adsorption efficiency of these oxides is important to investigate since iron oxides are generally incorporated with aluminum with a significant proportion [8]. Masue et al. [4] also stated that when Al was substituted within iron hydroxides, the rate of reductive dissolution of iron hydroxide decreased; hence, the redox reactions of iron oxides slow down during arsenic remediation.

Statistical experimental design technique is a useful approach for examining adsorption phenomena

*Corresponding author.

with mathematical models since more effort should be made to determine the influences of adsorption process variables and their interactions on the removal efficiency. The objective of designing an empirical study is to collect the maximum amount of relevant information with minimum expenditure of time and resources [9]. Application of this technique in the evaluation of adsorption process could result in improved product yields, closer confirmation of the output response to nominal and target requirements, and reduced number of experiments [10]. Response surface method (RSM) is one of the statistical approaches for improving an empirical model of the process and obtaining a certain estimate of optimum operating conditions [11]. Box-Behnken design is a second-order response surface model based on three-level incomplete factorial designs having points lying on the surface of a sphere surrounding the center of the design [12].

Although the design of the experiment techniques have been widely studied to find optimum adsorption process parameters [2, 13–16], there is no systematic study related to the response surface modeling of arsenate removal by binary oxides-enriched natural zeolite. To our knowledge, this is the first research addressing the arsenic adsorption potential of bimetallic oxides supported on Turkish clinoptilolite. The main objectives of the present study are application of a three-factor, three-level Box–Behnken experimental design for maximizing As(V) removal by binary oxides-doped natural clinoptilolite and examination of the interactive effects of three independent variables (i.e. solution pH, temperature, and initial concentration) on As(V) adsorption capacity.

2. Materials and methods

2.1. Reagents

All chemicals/reagents used in this work were of analytical reagent grade. Ferric chloride ($\text{FeCl}_3 \cdot 6\text{H}_2\text{O}$), anhydrous aluminum chloride (AlCl_3), and sodium hydroxide (NaOH) were purchased from Sigma–Aldrich.

2.2. Preparation of Fe/Al impregnated clinoptilolite

It was shown in our previous work [17] that the pretreated zeolites exhibited low or no adsorption capacities for As(V). However, major increases in As(V) uptake were observed for metal oxide-coated zeolites, especially for bimetallic oxides-coated ones. For that reason, the present study aimed to explore

arsenic adsorption onto iron-aluminum binary oxide-doped natural zeolites in detail. Clinoptilolite used in the present work was obtained from the Gördes-Manisa region of Turkey. In order to improve the ion exchange capacity, raw clinoptilolite was added to 2 mol L^{-1} of NaCl solution and the suspension was shaken for 24 h. Then, the treated sample was washed with distilled water to remove Cl^- ions and dried at 100°C . This sample was denoted as ZNa. Ten grams of ZNa was treated with a mixture of AlCl_3 and FeCl_3 solutions (1 mol L^{-1} concentration in total, 1:1) and 5 mol L^{-1} of NaOH was added dropwise to the suspension till pH reached 10–11. The Fe/Al impregnated zeolites were placed in a column and washed with distilled water until pH value became neutral. The resultant sample was dried at 65°C and named ZNa-AlFe.

2.3. Characterization

The FTIR spectrum was recorded with Perkin Elmer Spectrum One using attenuated total reflectance method. XRD measurement was performed on Philips Analytical X'Pert Pro X-ray diffractometer using $\text{Cu K}\alpha$ radiation. The specific surface area and pore-size distribution were calculated from Brunauer, Emmet, and Teller (BET) and Barrett-Joyner-Halenda (BJH) methods, respectively. Calculations were performed using Autosorb 1 software provided by Quantachrome instruments. The surface morphology of modified zeolite was analyzed by scanning electron microscopy (Philips XL30 SFEG). Zeta potential was determined from electrophoretic mobility by using Zetasizer 3000HSA. Potentiometric titration data were obtained using the method described by Helfferich [18]. Transmission electron microscopy (TEM) observations were performed with a high-resolution electron microscope (FEI Tecnai G2 F20 X-Twin) operated at 200 kV. The sample was prepared by dispersing in acetone and applying a few drops of the dispersion on Cu grid.

2.4. Experimental procedure

As(V) stock solution was prepared by dissolving $\text{Na}_2\text{HAsO}_4 \cdot 7\text{H}_2\text{O}$ in distilled water. The required amount of adsorbent was added to 25 mL of As(V) solution with different concentrations (0.5, 5.0, and 9.5 mg L^{-1}) at different pHs (3.0, 5.0, and 7.0) and temperatures (25, 45, and 65°C). During the adsorption experiments, the pH of solutions was kept constant by using diluted HCl or NaOH twice in a day. The determination of arsenic was performed by atomic absorption spectrophotometer (Analytic Jena ContraAA 700 TR). Analyses were conducted at a wavelength of

193.7 nm by a graphite furnace system using Pd/Mg (NO₃)₂ as a matrix modifier. Dilution was made with 2% HNO₃ solution and samples were reanalyzed in case the relative standard deviation exceeded 5%. All the experiments were carried out in triplicate and average results were reported. The As(V) adsorption capacity (q_e) was calculated from the following equation:

$$q_e = \frac{(C_i - C_e) \times V}{m} \quad (1)$$

where V is the volume of the solution (L), m is the adsorbent dosage (g), and C_i and C_e are the initial and equilibrium As(V) concentration (mg L⁻¹), respectively.

2.5. Response surface methodology

RSM is a collection of statistical and mathematical techniques for empirical model building and optimization of several process parameters by minimum number of experiments. RSM also offers a relationship between the controllable input parameters and response function.

Box–Behnken design is a spherical design based on three-level incomplete factorial designs including a central point and the middle points of the edges of the cube surrounded by the sphere [19]. Among the RSM designs (central composite (CCD), Doehlert matrix (DM), and three-level full factorial design), BBD and DM are more efficient than the CCD and much more efficient than the three-level full factorial designs [20]. On the other hand, the BBD requires less runs than the others, allowing calculations of the response function at intermediate levels.

In the present study, the BBD methodology was used in order to examine the effect of selected process variables: pH (3.0–7.0), temperature (25–65°C), and initial As(V) concentration (0.5–9.5 mg L⁻¹). Table 1 shows the range and levels of three independent reaction conditions. The empirical quadratic model was defined by three parameters: pH (x_1), temperature

(x_2), and initial As(V) concentration (x_3). The As(V) adsorption capacity of ZNa-AIFe (mg g⁻¹) was designated as dependent variable (Y_i). A class of three-level factorial designs in a second-order polynomial model was developed using “STATISTICA” (Ver. 8.0, StatSoft Inc., USA) software package.

The optimization procedure involves: (1) developing a mathematical model that best describes the adsorption process, (2) investigating the distribution of residuals of statistically designed combinations by Anderson–Darling normality test [21], (3) evaluating the quadratic approximation of BBD model with 95% confidence limits ($\alpha=0.05$), and (4) determination of statistical significance of each independent variable by Student’s t -test, lack of fit tests, and F - and p -values.

3. Results and discussion

3.1. Characterization studies

Table 2 shows the characteristic properties of the ZNa-AIFe sample. The surface area was found as 28.91 m² g⁻¹ and the total pore volume value was 0.166 cm³ g⁻¹. The isoelectric point (IEP) and the point of zero charge (PZC) values of ZNa-AIFe were obtained as 4.56 and 5.12, while the pH_{IEP} and pH_{PZC} of ZNa were found as 2.12 and 6.73, respectively [17]. The electrophoretic measurements revealed that the surface of ZNa was negatively charged even at acidic and neutral pHs whereas the surface of ZNa-AIFe was positive. It can be clearly seen that modification of (ZNa) with metal oxides caused a raise in positive potential of particle surface which could be the result of Fe/Al oxide forms [17].

The electrophoretic measurements indicated that the surface of electrostatic attraction may occur between positively charged ZNa-AIFe surface and for anionic species at pH < pH_{IEP}/pH_{PZC}. Dissociation of surface groups on the metal oxide-modified zeolite (inner and outer Helmholtz planes) due to the IEP values can be described [22] according to Eqs. (2)–(5):

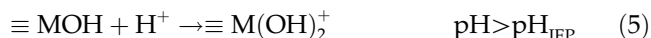
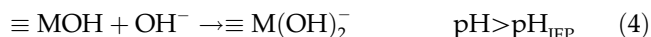
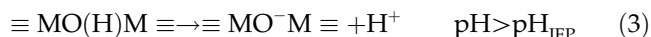


Table 1
Independent variables and levels of each factor for Box–Behnken

Variables	Symbol	Level		
		Low (−1)	Middle (0)	High (+1)
pH	x_1	3.0	5.0	7.0
Temperature	x_2	25	45	65
Initial As(V) concentration	x_3	0.5	5.0	9.5

Table 2
Characterization of ZNa-AIFe sample

Specific surface area, S_{BET}	(m ² g ⁻¹)	28.91
Micropore surface area, S_{BETmicro}	(m ² g ⁻¹)	60.64
Total pore volume, V_a	(cm ³ g ⁻¹)	0.166
Micropore volume, V_{micro}	(10 ⁻³ cm ³ g ⁻¹)	0.35
pH _{IEP}		4.56
pH _{PZC}		5.12



where M could be neutral (FeOH/AlOH), protonated (FeOH₂⁺/AlOH₂⁺), or hydroxylized (FeO⁻/AlO⁻) iron and aluminol sites. Moreover, other species present on the structure, such as Al(OH)₃, AlOH²⁺, Al₁₃O₄(OH)₂₄⁷⁺, and Al(OH)₄⁻, might also emerge in the adsorption process [17].

The FTIR spectrum of raw (ZNa) and bimetal oxide-impregnated zeolite (ZNa-AlFe) is shown in Fig. 1. Strong vibrations at about 1,050–1,150 cm⁻¹ are the indicators of asymmetric stretching of Si–O(Si) and Si–O(Al) vibrations in tetrahedral or alumino/silica-oxygen bridges [23,24]. The bands at about 1,614–1,650 cm⁻¹ indicate the H₂O deformation mode [25]. Vibration modes appearing near 3,400–3,500 cm⁻¹ are assigned to the bridging OH groups of silanol/aluminal active sites (≡Si–OH–Al≡, ≡Al–OH, ≡Si–OH) or OH⁻ groups of molecular water [26]. For the ZNa-AlFe sample, the vibrations increase due to the OH⁻ groups of Fe/Al oxides (Fe–OH, Fe–(OH)₂, FeO(OH), or AlOOH). Furthermore, lepidocrocite [γ-FeO(OH)] or goethite [α-FeO(OH)] forms represent vibrations near 640–775 cm⁻¹ [8].

The XRD patterns of ZNa and ZNa-AlFe samples indicated differences in the intensity of reflections. For both samples, the clinoptililite was the major crystalline phase detected on the pattern, as shown in Fig. 2. The peaks at 2θ = 9.875, 10.04, 11.19, 12.34, 13.047, 16.04, 22.342, 23.92, 27.04, 29.88, 16.907, 30.054, and 33.575 were found to be in good agreement with the data of clinoptililite (Joint Committee on Powder

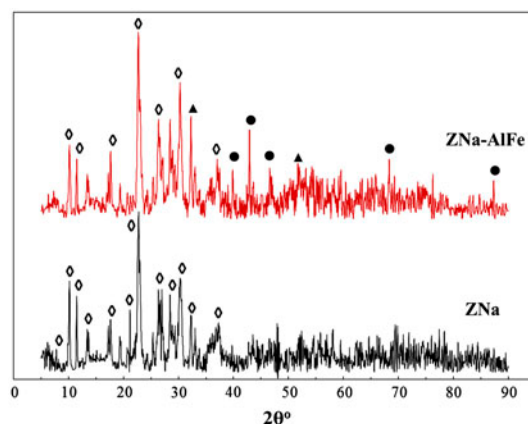


Fig. 2. XRD patterns of ZNa and ZNa-AlFe samples (◇: Clinoptililite, ●: Goethite, ▲: Lepidocrocite).

Diffraction Standards JCPDS-39-1,383). After modification with bimetallic oxides, new and sharp peaks (2θ = 37.02, 38.98, 42.88, 68.3, and 89.2) were observed at the ZNa-AlFe sample indicating the possibility of goethite or lepidocrocite phases. There was no significant peak detected for Al oxides attributing to the presence of noncrystalline aluminum hydroxide.

Scanning electron micrographs of ZNa and ZNa-AlFe samples are shown in Fig. 3. The ZNa sample had characteristic morphology of zeolites (Fig. 3 (a)); however, after modification the oxide particles aggregated on its surface (Fig. 3(b)). The TEM image of ZNa-AlFe (Fig. 4) represented rod-like crystals indicating the possibility of α-FeOOH or β-FeOOH forms [27]. TEM-EDX analysis revealed that Fe (3.87% wt.) and Al (4.59% wt.) were distributed on the zeolite surface.

3.2. Development of regression model and statistical analysis

In order to develop an optimum correlation between factors and response, linear, quadratic, interactive, and cubic models were applied to the experimental data. Lack of fit test was used to find an adequate model to predict the observed data. In the analysis of variance (ANOVA) table, if lack of fit *p*-value is greater than 0.05, the model is considered as valid. Table 3 gives the adequacy of the tested models. The quadratic model was found to be more significant with *p*-values for lack of fit (*p* = 0.078 for ZNa-AlFe). The coefficient of determination (*R*²) value was found to be 0.9977, indicating that the quadratic model fitted well and was chosen for further analysis.

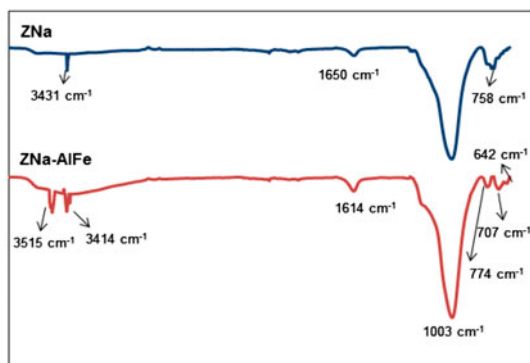


Fig. 1. FTIR spectrum of samples.

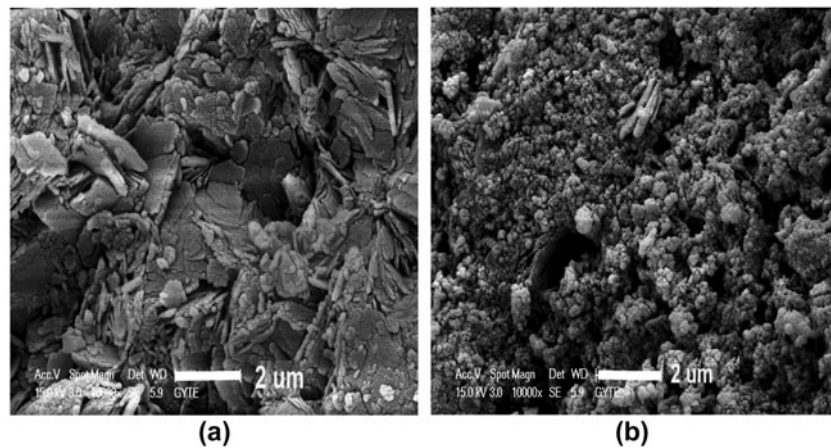


Fig. 3. SEM micrograph of (a) ZNa (b) ZNa-AlFe.

The experimental and predicted response data (Table 4 and Fig. 5) were observed to be in good agreement. Adsorption capacities of ZNa-AlFe varied between 0.1 and 6.6 mg g⁻¹. The Fe/Al oxide-impregnated zeolite was found to be an effective adsorbent compared to raw zeolite obtained by other researchers [4,28].

The normal probability plot of residuals is a diagnostic graphic to detect the deviations from the assumptions that errors are distributed homogeneously or not. Anderson-Darling normality test

rejects the hypothesis of normality when p -value is less than or equal to 0.05 and A^2 is greater than the critical value, which is 0.787 at 95% confidence level. The plot of normal probability of ZNa-AlFe (Fig. 6) indicated that there was no apparent deviation from normality according to the calculated A^2 (0.2801) and p (0.6441) values.

Table 5 gives the ANOVA results of the response surface model of As(V) adsorption onto ZNa-AlFe. Results were checked by probability (p) value, R^2 , and R^2_{Adj} values. The results indicated that interactions of

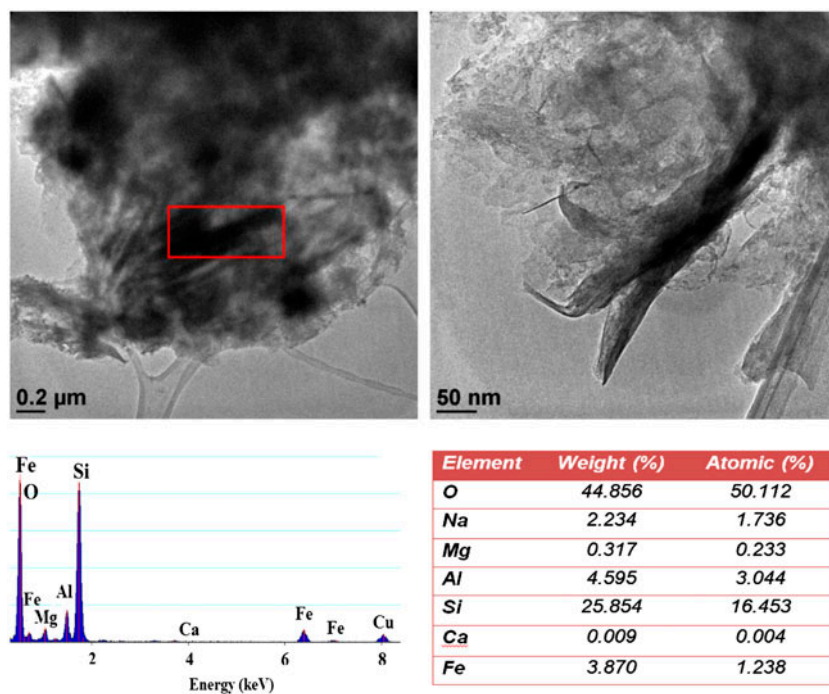


Fig. 4. TEM images and EDX analysis.

Table 3
Adequacy of the tested models

	Sum of squares	df	Mean square	F-value	p-value
<i>Lack of fit tests</i>					
Linear	6.83279	9	0.75920	101.301	0.000234
2FI	6.38586	6	1.06431	142.012	0.000130
Quadratic	0.11126	3	0.03709	4.948	0.078237
Cubic	0.000	0			
<i>Model summary statistics</i>					
	R^2	R^2_{Adj}			
Linear	0.88944	0.86393			
2FI	0.89664	0.83463			
Quadratic	0.99772	0.99480			
Cubic	0.99952	0.99807			

pH, temperature, and concentration were significant since p -values were less than the chosen significance level of 0.05. The values of $F_{ZNa-AlFe}$ (341.23) and R^2 (0.99772) revealed the accuracy and general availability of the model. The value of R^2_{Adj} was obtained as 0.9948, indicating high correlation between the observed and the predicted values.

The Pareto chart (Fig. 7) presents the effects of the independent variables and their interactions on the As

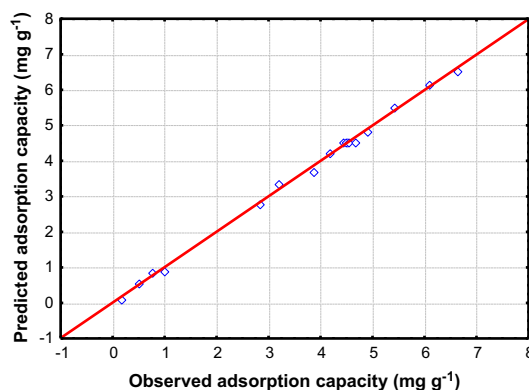


Fig. 5. Correlation of actual and predicted As(V) adsorption capacity.

(V) adsorption capacity. The magnitude of the t values reveals the significance of corresponding parameter in the regression model. As can be shown in Pareto chart, the linear term of initial concentration (x_3) ($t=84.128$) was found to be the most effective variance affecting arsenic adsorption. Quadratic term of concentration (x_3^2) and pH (x_1^2) showed favorable effect on adsorption capacity. The term x_1x_2 was not significant in the prediction of adsorption efficiency ($p=0.7625$).

Table 4
Observed and predicted sorption capacities

Run	Independent variables						As(V) sorption capacity (mg g^{-1})	
	pH, x_1		Temperature, x_2		Concentration, x_3		ZNa-AlFe	
	Coded	Actual	Coded	Actual	Coded	Actual	Observed	Predicted
1	-1	3.0	-1	25.0	0	5.0	2.822	2.787
2	1	7.0	-1	25.0	0	5.0	3.872	3.709
3	-1	3.0	1	65.0	0	5.0	3.186	3.349
4	1	7.0	1	65.0	0	5.0	4.180	4.215
5	-1	3.0	0	45.0	-1	0.5	0.175	0.112
6	1	7.0	0	45.0	-1	0.5	0.499	0.565
7	-1	3.0	0	45.0	1	9.5	4.886	4.821
8	1	7.0	0	45.0	1	9.5	6.094	6.156
9	0	5.0	-1	25.0	-1	0.5	0.761	0.859
10	0	5.0	1	65.0	-1	0.5	0.992	0.892
11	0	5.0	-1	25.0	1	9.5	5.407	5.507
12	0	5.0	1	65.0	1	9.5	6.640	6.542
13	0	5.0	0	45.0	0	5.0	4.444	4.530
14	0	5.0	0	45.0	0	5.0	4.506	4.530
15	0	5.0	0	45.0	0	5.0	4.491	4.530
16	0	5.0	0	45.0	0	5.0	4.536	4.530
17	0	5.0	0	45.0	0	5.0	4.673	4.530

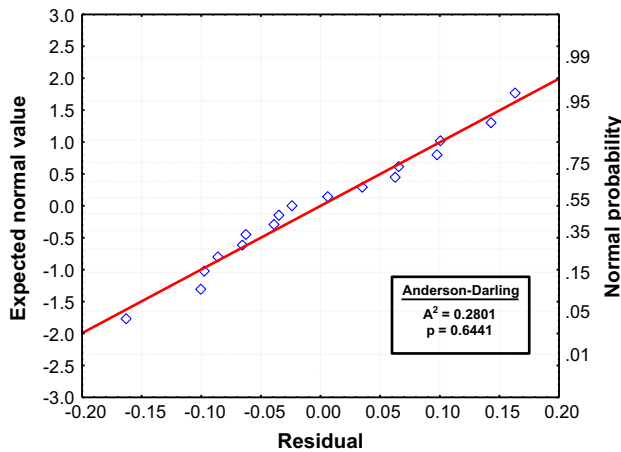


Fig. 6. Normal probability plot of residuals.

The BBD supplies an empirical relationship between the dependent and independent variables. The functional relationship between response (Y_i) and factors (x_i) can be approximated by the quadratic equation as follows:

$$Y_i = \beta_0 + \beta_1 x_1 + \beta_2 x_2 + \beta_3 x_3 + \beta_{12} x_1 x_2 + \beta_{13} x_1 x_3 + \beta_{23} x_2 x_3 + \beta_{11} x_1^2 + \beta_{22} x_2^2 + \beta_{33} x_3^2 \quad (6)$$

where β_0 is the constant, β_1 , β_2 , and β_3 are the coefficients of linear effect of the input factors, β_{11} , β_{22} , and β_{33} are the coefficients of quadratic effects, β_{12} , β_{13} , and β_{23} are the 2-way linear-by-linear interaction effects of independent parameters. Based on the

Table 5
ANOVA of As(V) sorption

Factors	Sum of squares	df	Mean square	F-value	p-value
Model	61.93	9	6.88	341.23	<0.0001
x_1	1.59803	1	1.59803	213.226	0.000128
x_1^2	2.53425	1	2.53425	338.148	0.000051
x_2	0.57031	1	0.57031	76.097	0.000951
x_2^2	0.24089	1	0.24089	32.142	0.004774
x_3	53.04243	1	53.04243	7077.514	0.000000
x_3^2	2.97670	1	2.97670	397.184	0.000037
$x_1 x_2$	0.00078	1	0.00078	0.105	0.762569
$x_1 x_3$	0.19514	1	0.19514	26.038	0.006969
$x_2 x_3$	0.25100	1	0.25100	33.491	0.004430
Lack of fit	0.11126	3	0.03709	4.948	0.078237
Pure error	0.02998	4	0.00749		
Total SS	62.07353	16			
$R^2 = 0.99772$; $R^2_{Adj} = 0.9948$					

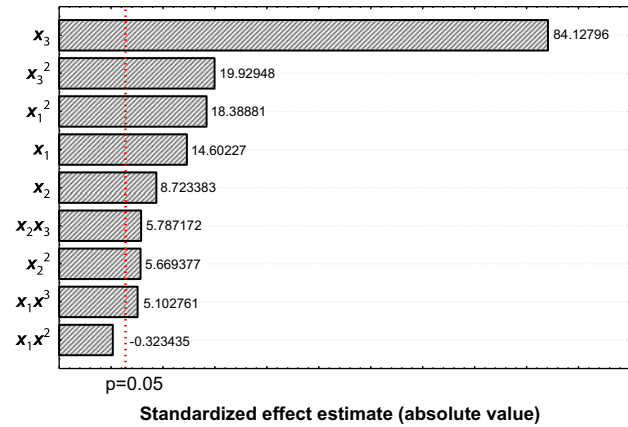


Fig. 7. Pareto chart of variables and their interactions.

regression coefficients, the empirical equation of ZNa-AlFe was described by neglecting the insignificant effect ($x_1 x_2$):

$$q_{ZNa-AlFe} = -5.6687 + 1.9837 x_1 - 0.04817 x_2 - 0.0005 x_2^2 + 0.7283 x_3 - 0.04041 x_3^2 + 0.02454 x_1 x_3 + 0.00278 x_2 x_3 \quad (7)$$

3.3. Effects of process variables on As(V) adsorption

The three-dimensional (3D) response surface plots are the best way to examine the interactions between the factors and response. Hence, in the present study, 3D surface plots were constructed in order to understand the effects of variables and their interactions (Fig. 8(a)–(c)).

3.3.1. Effect of solution pH

The relation between the solution pH and the removal capacity of ZNa-AlFe adsorbent is presented in Fig. 8(a) and (c). The adsorption efficiency increased with pH ranging from 3.0 to 5.5. At any pH above 6.0, the adsorption capacity decreased slightly. The capacity was obtained as 3.186 mg g^{-1} at pH 3.0 (Run #3) while it raised to 4.180 mg g^{-1} at pH 7 (Run #4). When solution pH was 3, As(V) removal could be through electrostatic attractions between H_2AsO_4^- and Al/FeOH_2^+ ions. As pH was increased above the pH_{PZC} ($\text{pH}_{\text{PZC}} = 5.12$), adsorption increased. This could be attributed to the strong surface complexation reactions between terminal aluminol/iron oxide groups and As(V) ions [29,30].

3.3.2. Effect of temperature

As shown in Fig. 8(a) and (b), increasing the temperature had a favorable effect on As(V) adsorption efficiency. The As(V) adsorption capacity increased gradually from 5.407 mg g⁻¹ at 25°C (Run #11) to 6.640 mg g⁻¹ at 65°C (Run #12). The enhancement of adsorption capacity with increasing temperature might be attributed to the breaking of bonds on the adsorbent surface and increase in the diffusion rate of adsorbate ions across the external boundary layer and in the internal pores of the adsorbent [31].

3.3.3. Effect of initial concentration

Adsorption experiments were carried out at different initial As(V) concentrations ranging from 0.5 to 9.5 mg L⁻¹. The combined effects of initial As(V) concentration with temperature and pH are visualized in Fig. 8(b) and (c). Initial As(V) concentration had a marked favorable and considerable effect on the amount of As(V) adsorbed onto ZNa-AlFe. The adsorption capacities were found to be 0.175 (Run #5) and 4.886 mg g⁻¹ (Run #7) for initial As(V) concentration of 0.5 and 9.5 mg L⁻¹, respectively. This phenomenon might be explained by higher driving force to overcome mass transfer resistance between adsorbate and adsorbent [32] or by increase in the number of available sites on the surface with increasing temperature [31].

3.4. Model confirmation experiments

According to the optimum predicted critical values, a series of three-point calibration studies was conducted. Table 6 presents the model confirmation results at optimum point of independent factors. The predicted adsorption capacity of ZNa-AlFe was found to be 6.81 mg g⁻¹ and experimental capacity was obtained as 6.62 mg g⁻¹. Model validation experiments

Table 6
Model validation

Sample	pH	Temperature (°C)	Concentration (mg L ⁻¹)	Capacity (mg g ⁻¹)	
				Predicted	Experimental
ZNa-AlFe	6.01	62.48	9.43	6.81	6.67 ± 0.25

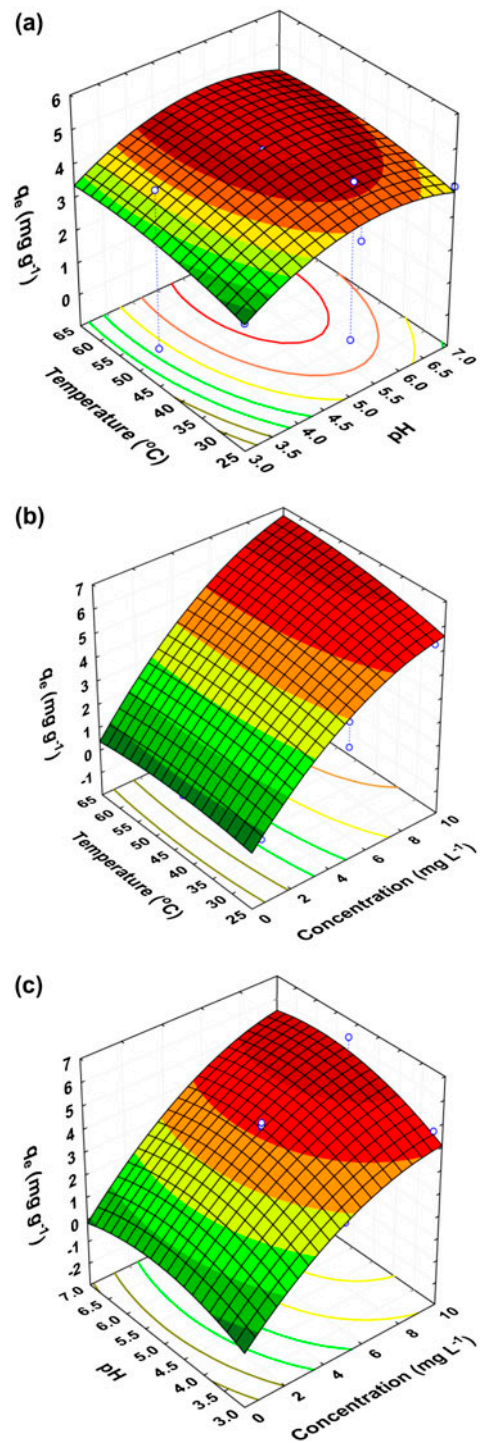


Fig. 8. Response surfaces for combined effect of (a) temperature and pH at constant initial concentration of 5 mg L⁻¹; (b) initial concentration and temperature at constant pH of 5.0; and (c) pH and initial concentration at constant temperature of 25°C on the adsorption capacity of ZNa-AlFe.

indicated that the applied method meets the criteria set for responses and it could be further employed to determine the significance for As(V) adsorption onto ZNa-AlFe. Furthermore, according to the obtained optimum conditions, the RSM investigation method can be used especially for the treatment of arsenic-contaminated groundwaters owing to geothermal activities. Geothermal waters may include high level of arsenic concentrations. There have been several studies reported in the literature about arsenic contamination levels which were similar to the optimum conditions found in the previous study [1,33–35].

4. Conclusions

RSM by BBD was used to examine the role of three process parameters on As(V) adsorption capacity. Solution pH, temperature, and initial concentration were selected as independent variables. The response function was the As(V) adsorption capacity of ZNa-AlFe sample. The quadratic model was found highly to be significant according to the lack of fit test and provided the best fit to the experimental data with high p -value of lack of fit ($p=0.078$). Therefore, for further analysis the quadratic model was chosen. Anderson–Darling test demonstrated that residuals were normally distributed and the error variance was homogeneous. ANOVA results indicated that the linear term of initial concentration ($t=84.13$) was found to be more effective than other variances. The empirical equation of adsorption capacity ZNa-AlFe (Eq. 7) was established and it could be further employed in the chosen range to find the adsorption capacity without any experimental study. The quadratic form of concentration and pH showed favorable effect on adsorption capacity, while the interaction of pH and temperature was not significant in the prediction of adsorption efficiency ($p=0.76$). Solution pH of 6.0 and initial concentration of 9.4 mg L^{-1} at 62.4°C were found as optimum combination of process parameters. Higher adsorption capacities were achieved with increasing temperature, indicating the endothermic behavior of the process.

According to the results of the present study, it can be concluded that the iron-aluminum binary oxide-doped clinoptilolite has the potential to be used as environmental benign, abundant, inexpensive, and effective adsorbent for removing As(V) from aqueous media. As Turkey is one of the major producers of zeolites, the preparation of the hybrid adsorbent by

using natural zeolite will also contribute to the economy of the country.

References

- [1] K.R. Henke, Introduction, in: K.R. Henke, Arsenic Environmental Chemistry Health Threats and Waste Treatment, Wiley, New York, 2009, pp.1–5.
- [2] M. Bilici Baskan, A. Pala, A statistical experiment design approach for arsenic removal by coagulation process using aluminum sulfate, *Desalination* 254 (2010) 42–48.
- [3] X. Dou, Y. Zhang, B. Zhao, X. Wu, Z. Wu, M. Yang, Arsenate adsorption on an Fe–Ce bimetal oxide adsorbent: EXAFS study and surface complexation modeling, *Colloids Surf., A* 379 (2010) 109–115.
- [4] Y. Masue, R.H. Loeppert, T. Kramer, Arsenate and arsenite adsorption and desorption behavior on coprecipitated aluminum:iron hydroxides, *Environ. Sci. Technol.* 41 (2007) 837–842.
- [5] H.J. Hong, W. Farooq, J.S. Yang, J.W. Yang, Preparation and evaluation of Fe & Al binary oxide for arsenic removal: Comparative study with single metal oxides, *Sep. Sci. Technol.* 45 (2010) 1975–1981.
- [6] J. Silva, J.W.V. Mello, M. Gasparon, W.A.P. Abrahão, V.S.T. Ciminelli, T. Jong, The role of Al-Goethites on arsenate mobility, *Water Res.* 44 (2010) 5684–5692.
- [7] D.E. Giles, M. Mohapatra, T.M. Issa, S. Anand, P. Singh, Iron and aluminium based adsorption strategies for removing arsenic from water, *J. Environ. Manage.* 92 (2011) 3011–3022.
- [8] R.M. Cornell, U. Schwertmann, *The Iron Oxides: Structure, Properties, Reactions, Occurrence and Uses*, Wiley, Weinheim, 2003.
- [9] Z.R. Lazić, *Design of Experiments in Chemical Engineering*, WILEY-VCH, Weinheim, 2004.
- [10] D. Kavak, Removal of boron from aqueous solutions by batch adsorption on calcined alunite using experimental design, *J. Hazard. Mater.* 163 (2009) 308–314.
- [11] D.C. Montgomery, *Design and Analysis of Experiments*, 7th ed., John Wiley & Sons, Hoboken, 2008.
- [12] P. Tripathi, V.C. Srivastava, A. Kumar, Optimization of an azo dye batch adsorption parameters using Box–Behnken design, *Desalination* 249 (2009) 1273–1279.
- [13] M. Ciopec, C.M. Davidescu, A. Negrea, I. Grozav, L. Lupa, P. Negrea, A. Popa, Adsorption studies of Cr(III) ions from aqueous solutions by DEHPA impregnated onto Amberlite XAD7—Factorial design analysis, *Chem. Eng. Res. Des.* 90 (2012) 1660–1670.
- [14] Y. Safa, H.N. Bhatti, Biosorption of Direct Red-31 and Direct Orange-26 dyes by rice husk: Application of factorial design analysis, *Chem. Eng. Res. Des.* 89 (2011) 2566–2574.
- [15] K. Yetilmezsoy, S. Demirel, R.J. Vanderbei, Response surface modeling of Pb(II) removal from aqueous solution by Pistacia vera L.: Box–Behnken experimental design, *J. Hazard. Mater.* 171 (2009) 551–562.
- [16] A. Arami-Niya, W.M.A.W. Daud, F.S. Mjalli, F. Abnisa, M.S. Shafeeyan, Production of microporous palm shell based activated carbon for methane adsorption: Modeling and optimization using response surface methodology, *Chem. Eng. Res. Des.* 90 (2012) 776–784.
- [17] E. Bilgin Simsek, E. Özdemir, U. Beker, Zeolite supported mono- and bimetallic oxides: Promising adsorbents for removal of As(V) in aqueous solutions, *Chem. Eng. J.* 220 (2013) 402–411.
- [18] F. Helfferich, *Ion Exchange*, Dover, New York, NY, 1995.
- [19] G.E.P. Box, D.W. Behnken, Some new three-level designs for the study of quantitative variables, *Technometrics* 2 (1995) 455–475.

- [20] S.L.C. Ferreira, R.E. Bruns, H.S. Ferreira, G.D. Matos, J.M. David, G.C. Brando, E.G.P. da Silva, L.A. Portugal, P.S. dos Reis, A.S. Souza, W.N.L. dos Santos, Box–Behnken design: An alternative for the optimization of analytical methods, *Anal. Chim. Acta* 597 (2007) 179–186.
- [21] R.L. Anderson, *Practical Statistics for Analytical Chemists*, Van Nostrand Reinhold, New York, NY, 1987.
- [22] V.M. Gunko, V.I. Zarko, R. Lebeda, E. Chibowski, Aqueous suspension of fumed oxides: Particle size distribution and zeta potential, *Adv. Colloid Interface Sci.* 91 (2001) 1–112.
- [23] J.A. Lercher, A. Jentys, Infrared and Raman spectroscopy for characterizing zeolites, in: J. Čejka, H. van Bekkum, A. Corma, F. Schüth (Eds.), *Introduction to Zeolite Science and Practice*, 3rd Revised Edition, Elsevier, Amsterdam, 2007, pp. 435–476.
- [24] M.M. Dávila-Jiménez, M.P. Elizalde-González, J. Mattusch, P. Morgenstern, M.A. Pérez-Cruz, Y. Reyes-Ortega, R. Wennrich, H. Yee-Madeira, *In situ* and *ex situ* study of the enhanced modification with iron of clinoptilolite-rich zeolitic tuff for arsenic sorption from aqueous solutions, *J. Colloid Interface Sci.* 322 (2008) 527–536.
- [25] V.S. Somerset, L.F. Petrik, R.A. White, M.J. Klink, D. Keyb, E. Iwuoha, The use of X-Ray fluorescence (XRF) analysis in predicting the alkaline hydrothermal conversion of fly ash precipitates into zeolites, *Talanta* 64 (2004) 109–114.
- [26] M.K. Doula, Synthesis of a clinoptilolite–Fe system with high Cu sorption capacity, *Chemosphere* 67 (2007) 731–749.
- [27] U. Schertzmann, R.M. Cornell, *Iron Oxides in the Laboratory*, VCH, Weinheim, 2000.
- [28] R.G. Robins, P. Singh, R.P. Das, in: R.G. Reddy, V. Ramachandran, TMS (The Minerals, Metals & Materials Society), ISBN 0-87339-585-9, 2005.
- [29] W. Qui, Y. Zheng, Arsenate removal from water by an alumina-modified zeolite recovered from fly ash, *J. Hazard. Mater.* 148 (2007) 721–726.
- [30] Y. Arai, E.J. Elzinga, D.L. Sparks, X-ray absorption spectroscopic investigation of arsenite and arsenate adsorption at the aluminum oxide–water interface, *J. Colloid Interface Sci.* 235 (2001) 80–88.
- [31] Y. Wen, Y. Wu, Optimizing Adsorption of Co(II) and Ni(II) by 13× molecular sieves using response surface methodology, *Water, Air, Soil Pollut.* 223 (2012) 6095–6107.
- [32] E. Malkoc, Y. Nuhoglu, Potential of tea factory waste for chromium (VI) removal from aqueous solutions: Thermodynamic and kinetic studies, *Sep. Purif. Technol.* 54 (2007) 291–298.
- [33] World Health Organization, *United Nations Synthesis Report on Arsenic in Drinking Water*, Geneva, 2001.
- [34] S. Wang, C.N. Mulligan, Occurrence of arsenic contamination in Canada: sources, behavior and distribution, *Sci. Total Environ.* 366 (2006) 701–721.
- [35] L. Altaş, M. Işık, M. Kavurmacı, Determination of arsenic levels in the water resources of Aksaray Province, Turkey, *J. Environ. Manage.* 92 (2011) 2182–2192.